# Morphology and Grain Texture in As-Deposited and Heat Treated Inconel 718 Structures Produced using Laser-Based Powder Bed Fusion

David B. Saint John[*], Sanjay B. Joshi[*], Timothy W. Simpson[*],
Meng Qu[†], John David Rowatt[†], and Yucun Lou[†]
[*]Industrial & Manufacturing Engineering, Penn State University, University Park, PA 16802
[†]Mechanical & Materials Science, Schlumberger-Doll Research, Cambridge, MA 02139

## Abstract

With increasing interest in the use of powder bed fusion (PBF) processes for additive manufacturing, understanding the relationship between as-deposited and heat treated states and the intrinsic anisotropy of fabricated parts has become critical for its successful application. This phenomenon has been studied and reported extensively for Inconel 718 parts fabricated using PBF for aerospace applications, but few reports exist on the morphology and grain texture of Inconel 718 parts fabricated for oil and gas applications, which have different demands. This work demonstrates that the anisotropy in Inconel 718 parts produced using laser-based PBF is not entirely removed by subsequent heat treatments, and it may be an artifact of the as-deposited grain structure, whose elongated grains may stretch through several melt pools. The as-built material is observed to exhibit some texturing, with (001) being the preferential growth direction. Despite some residual anisotropy, heat treatments are sufficient to provide material qualities that meet specification, even without the use of a HIP (hot isostatic pressing) step. It is hypothesized that similarly elongated grain structures may explain the anisotropy observed in other materials systems employed in PBF additive manufacturing processes.

## 1. Introduction and Motivation

While increasing effort is being directed toward the application of additive manufacturing (AM) processes for the production of full-service components, many concerns and unknowns continue to limit widespread application of the technology, particularly for metals. In particular, it has become apparent within the field of metal AM that in the material systems currently available for use, whether using powder bed fusion (PBF) processes or other metal AM approaches, many find that the as-built microstructure is undesirable or unsuitable without subsequent annealing [1] and in some cases may be undesirable even with annealing [2].

Given this awareness, the application of AM processes is currently hindered by the absence of data regarding suitable heat treatment steps required to achieve microstructures more comparable to those found in more traditional cast or wrought parts. The steps for optimization of AM materials are expected to include stress relief, solution annealing, aging, and possibly hot isostatic pressing (HIP) treatments whose temperatures and soak times are likely to be specific to each material and application. It may be that wrought heat treatments are adequate to refine the as-built microstructure of PBF parts, but this has yet to be demonstrated for all of the materials currently being used in PBF processes.

Direct Metal Laser Sintering (DMLS, a proprietary form of PBF offered by EOS GmbH) of Inconel 718 has seen increasing study [1] and application [3], but heat treatment reports in

literature have emphasized aerospace applications over those for the oilfield, whose heat treatment schedules have come to diverge [4,5]. The abrasive and corrosive nature of the downhole environment, as well as the need for non-magnetic alloys to minimize interference with measurement devices, imposes limitations on material suitability which Inconel 718 is able to satisfy [4]. Downhole instrumentation operates with a minimum of free space, and possible design optimization using AM is a significant driving factor which requires further assessment of material quality for safe application. This work seeks to demonstrate a heat treatment for PBF parts that exhibits mechanical and microstructural properties similar to that of wrought Inconel 718 manufactured under the 6A718 specification [6], which has been designed to optimize corrosion properties of 718 for hydrogen sulfide-rich environments [4,5,7]. This work adds to the growing body of literature investigating the microstructure and mechanical properties of Inconel 718 (e.g., [8,9]) but with an emphasis on oilfield applications rather than aerospace.

It is known that as-built PBF material exhibits significant anisotropy when comparing the in-plane and out-of-plane mechanical properties [1]. The degree to which this anisotropy is present in heat-treated PBF materials is not fully understood and requires further exploration. In reports on electron beam (E-beam) based PBF of Inconel 718 [10,11,12,13], strong texturing of grains has been observed, providing an additional mechanism for mechanical anisotropy beyond grain shape. Similar analysis of laser-based PBF Inconel 718 via DMLS has not been reported, and it is possible that the differences in cooling rates and thermal gradients between E-beam and laser-based PBF processes produce a different microstructure. We seek to quantify and explain the degree of anisotropy present before and after heat treatment of DMLS-fabricated IN718 components using an application-specific thermal schedule.

In this work, we assess grain elongation, shape, and texturing in Inconel 718 PBF materials, both as-built and after solution annealing and aging treatments meant to obtain microstructures acceptable for sour service, comparing these microstructural and associated mechanical properties with those expected of 6A718 material.

## 2. Experimental Procedures

In order to assess the mechanical and microstructure of both as-built and heat treated DMLS Inconel 718, a series of samples were produced using an EOS M280 PBF system, built using the OEM's standard parameters for Inconel 718 with a 40 micron layer height. Processing parameters remained fixed in each build in an effort to match commonly produced material. Feedstock powders consisted of mostly spherical, gas (argon) atomized, nominally Inconel 718 material with a mean particle size of 22.7 μm.

Sample specimens consisted of rectilinear blanks for tensile (0.6 cm x 0.6 cm x 5 cm) and Charpy specimens (1.1 cm x 1.1 cm x 5.6 cm), oriented both in-plane (X/Y-oriented or 'laying down') and out-of-plane (Z-oriented or 'standing up'). A screenshot of the build layout used can be seen in Figure 1, showing Charpy and tensile specimens as well as some additional samples. For microstructural analysis, both orientations were sampled, with Z-oriented samples measured at the top and bottom of the block in an effort to distinguish possible variance due to the thermal histories associated with build duration and/or build height.

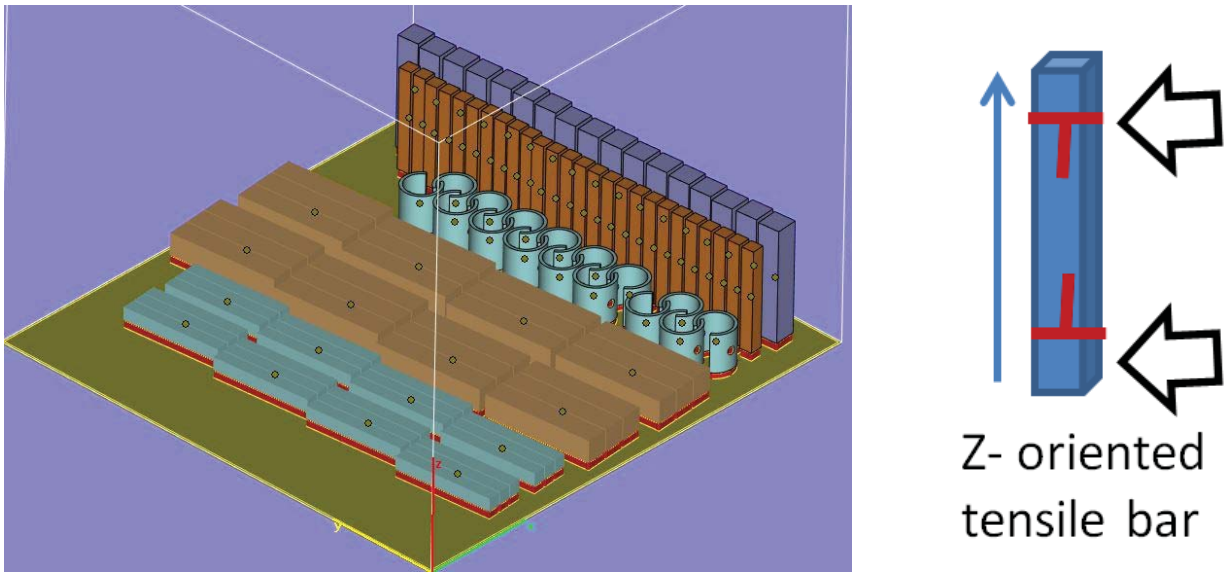


Figure 1: Isometric view of initial build layout showing tensile and Charpy specimens. Taller specimens are placed closer to the powder supply in an effort to avoid potential shorting during fabrication. Microstructural sampling was performed on tensile and Charpy specimens on both the top and bottom, obtaining views of both the X-Y plane and the X-Z growth face.

Our specimens were removed using wire electrical discharge machining (wire-EDM) prior to solution annealing and aging but without stress relief. Samples described within this study were subjected to solution annealing and aging treatments to modify the as-built microstructure. The solution annealing and aging conditions are chosen following the recommendations in literature for oil and gas Inconel 718 [4].

Specimens destined for mechanical testing were machined and tested to the specifications described in ASTM E8 and E23 by Westmoreland Mechanical Testing and Research, Inc in Youngstown, PA. All tests were performed at room temperature. Microstructural samples were sectioned, mounted, ground, and polished prior to etching. Electrolytic etching was applied to polished surfaces, by applying a potential of one volt to the surface while submerged in Oxalic acid (at a concentration of 10% by weight) for less than 1 second. It should be noted that the as-built material was significantly resistant to etching in comparison to any heat-treated material (wrought or PBF) and may require additional etching to provide adequate contrast for imaging.

Images were obtained from the samples using both optical microscopy and scanning electron microscopy (SEM), with electron backscatter diffraction (EBSD) used to determine the relative orientation of grains as a function of build direction. EBSD data was typically collected with a working voltage of 18-20 kV, using a beam current of 3.2 – 6.4 nA.

## 3. Results and Discussion

The mechanical property data obtained from tensile and Charpy measurements both as-built and heat treated samples is summarized in Figure 2, along with minimum requirements associated with the UNS N07718 120K (or N07716 120K, or N07725 120K) specifications. While the as-built material does not satisfy all of the requirements of these specifications

(particularly given the observed weakness in the Z-orientation), material in the heat treated condition exhibits mechanical behavior that achieves the specification and may be suitable for sour service where wrought material is currently in use.

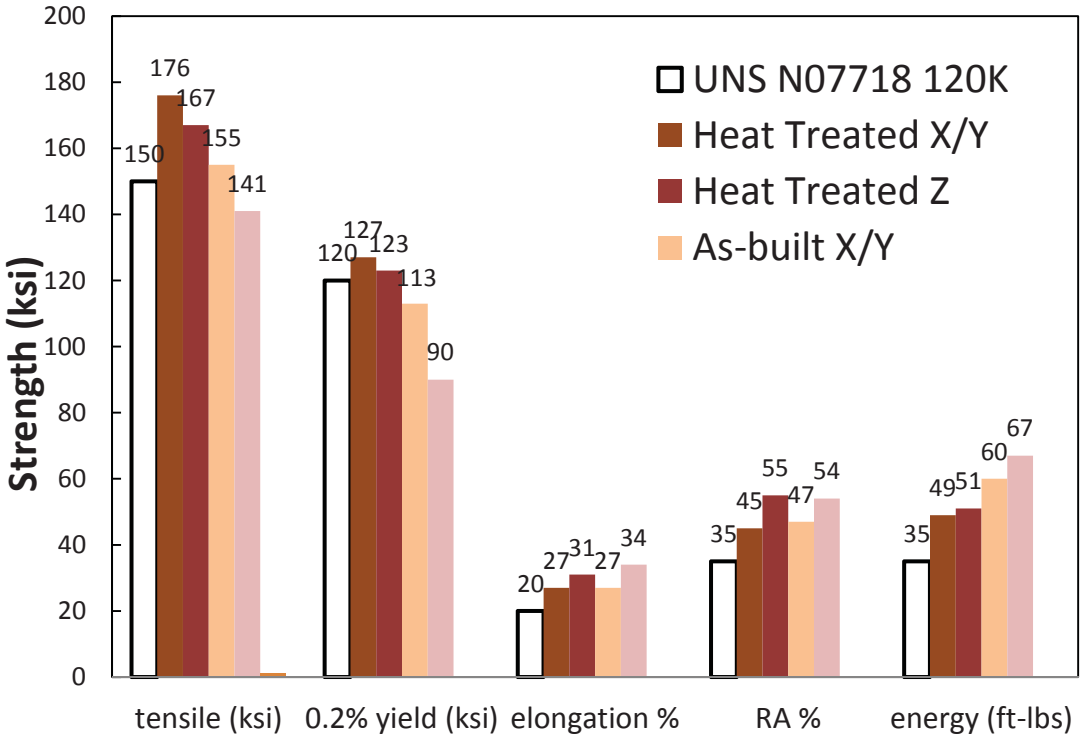


Figure 2. Summary of mechanical property data obtained from as-built and heat treated material, as compared to the 6A718 specification (UNS N07718 120K).

As reported in other studies (e.g., [1]), the tensile strength of as-built material is substantially anisotropic, with out-of-plane ultimate tensile strengths being ~ 90% of those measured in-plane, while the elongation and impact energy absorbed of in-plane samples are 79% and 89%, respectively, compared with those built out-of-plane. In the heat treated samples, this anisotropy persists to a lesser degree, as material pulled in the out-of-plane direction maintains ~95% of the ultimate tensile strength of comparable in-plane specimens, while the elongation and impact energy of the in-plane specimens rose to 87% and 96% of the out-of-plane samples following the application of heat treatments. While the elongation and reduced area (RA) do not substantially change with heat treatment, it is worth noting that the measured values satisfy requirements derived from wrought material, even given the residual anisotropy that remains. Meanwhile, the improvement in yield strength may be understood both as a refinement of the local microstructure (e.g., solutionizing of the Nb-rich Laves phase and precipitation of hardening phases) as well as a modification of grain size and shape, with the as-built elongated grains evolving toward a more isotropic (but still elongated) shape. These conclusions are supported by the variance in microstructure observed as a function of orientation and heat treatment conditions discussed next.

## 3.1. Microstructure of As-Built Material

The as-built microstructure of PBF In718 is shown in Figure 3. The observed microstructure is similar to those documented in literature [1]; however, the edge effects of the contour paths have not been shown previously. These can be seen for both in-plane and out-of-plane orientations in the optical micrographs shown in Figure 3, where the infill melt-pools can be distinguished from those of the contour melt-pools based on penetration depth. These contour melt-pools do not penetrate as deeply as those of the infill region, which might be expected given the variance in laser power from infill paths to contour paths.

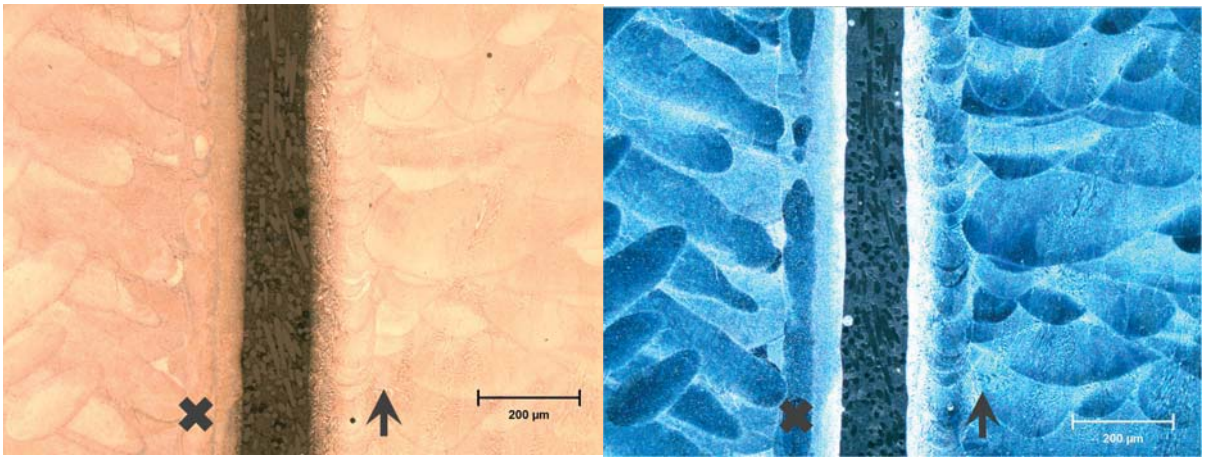


Figure 3: Bright- and dark-field optical micrographs comparing build directions in as-deposited DMLS material. The build orientation is indicated with an arrow, while the X denotes samples viewed within the build plane. Weld pools can be observed clearly, and the surface contour paths at the part edges are distinct from those of the fill pattern.

This as-built mesostructure appears basically homogenous throughout build thickness, with a microstructure similar to a fine-grained cast material [14,15], wherein a Nb/Mo-rich phase has precipitated/segregated from the FCC γ matrix. Energy dispersive spectroscopy (EDS) mapping confirms that the elemental segregation observed in PBF Inconel 718 is not unlike that observed in rapidly cooling cast material [15,16], with a spacing of 1-2 µm between the segregation regions (see Figure 4). Though there may be exceptions, the observed segregation phase appears to be coherent with the surrounding grain, giving some indication of grain orientation based on the symmetry and shape of the segregated phase. This may be compared with the microstructure of as-cast IN718, under the conditions of rapid cooling, when Laves phase segregation occurs [14,16,17].

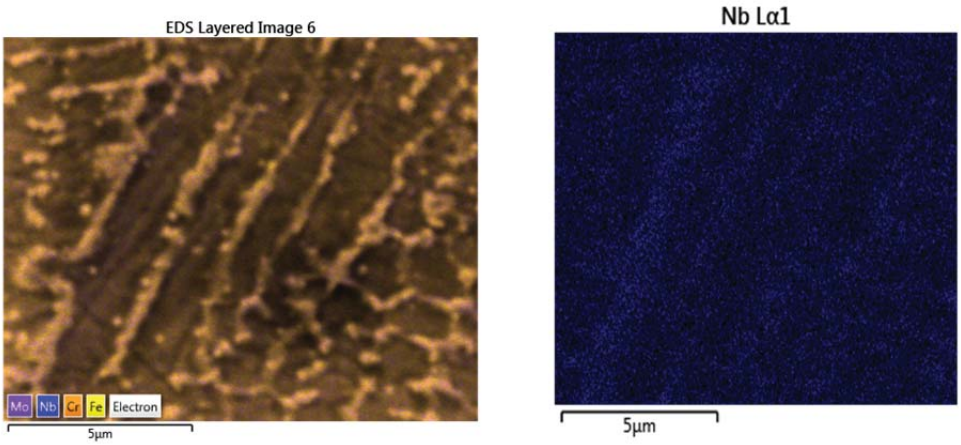


Figure 4: Segregated regions in solidification microstructures exhibit Nb enrichment (at 17.8 wt% compared to the 5.3 wt% in matrix), along with slight Cr and Fe deficiency (at 11.4 and 9.9 wt% respectively) as compared to surrounding material (with 19.0 and 17.6 wt% respectively).

The grain structure of the as-built material appears to be elongated or non-equiaxed, with roughly columnar/feathered grains 10-100 µm wide that extend throughout several melt pools (100-300 µm), as shown by the EBSD map in Figure 5. While there appears to be some preferential orientation in as-built material, this texturing does not appear as consistent as has been demonstrated in Inconel 718 processed using electron-beam PBF methods [10,11,12,13]. If texturing during solidification occurs in the <001> direction, then one would expect to see both a preference for <001> orientation from the out of plane orientation as well as a preference for orientations along the <001> to <011> directions within the X-Z growth plane. These effects can be seen in the EBSD maps shown in Figure 5, as little of the <111> orientation is observed in the X-Z plane, while the X-Y plane exhibits substantial <001>.

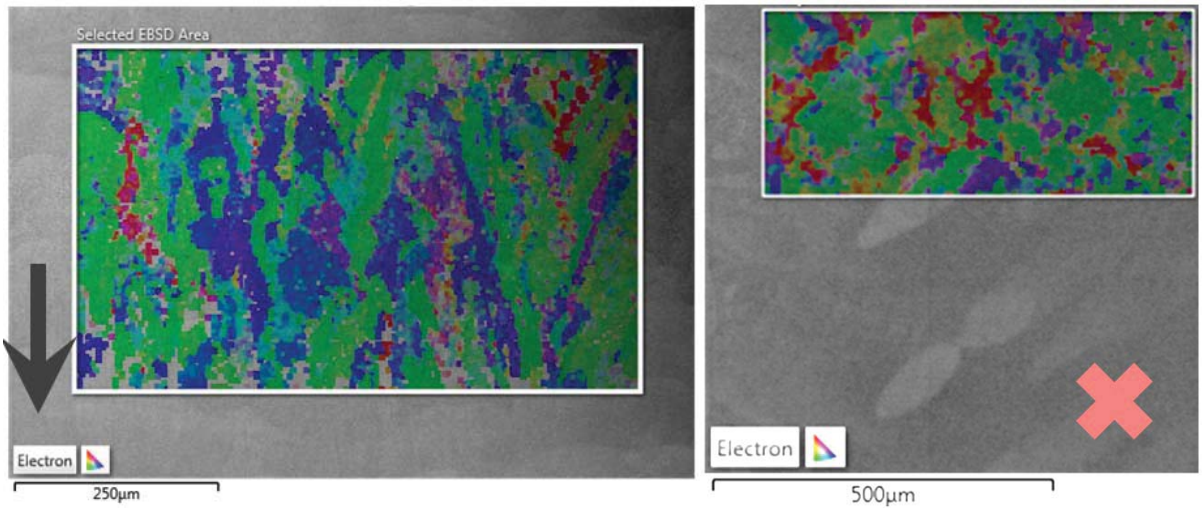


Figure 5 SEM and EBSD map of as-deposited material, showing IPF Z data. Extension of grains throughout weld pools is evident, with some degree of epitaxy occuring from later to layer. A preference for growth in the <001> direction can be seen by the predominance of green in the in-plane direction, and the predominance of <001> (green) and <011> (blue) in the out-of-plane direction. Scale bar = 250 µm. Build orientation is indicated with an arrow, while the X denotes samples viewed within the build plane.

Because the grains stretch throughout the melt pools, the contrast demarking the melt pool boundaries cannot be the result of grain boundaries, unlike the contrast typically observed in heat treated cast or wrought material. Instead, the source of contrast from the melt pools can be observed using intermediate magnifications and appears to result from a variance in the coarsening of the segregated phase. This variance can be seen in Figure 6, whose frame is dominated by two grains that extend on either side of a melt pool boundary. The upper and lower grains can be distinguished by the difference in the symmetry character of the segregated phase, while the boundary of the melt pool marks a difference in the relative fraction or size of the segregated phase. This might be accounted for by a local heat-affected zone (HAZ) effect, whereby the liquid melt pool exacerbates the segregation present in the solidified under-layer.

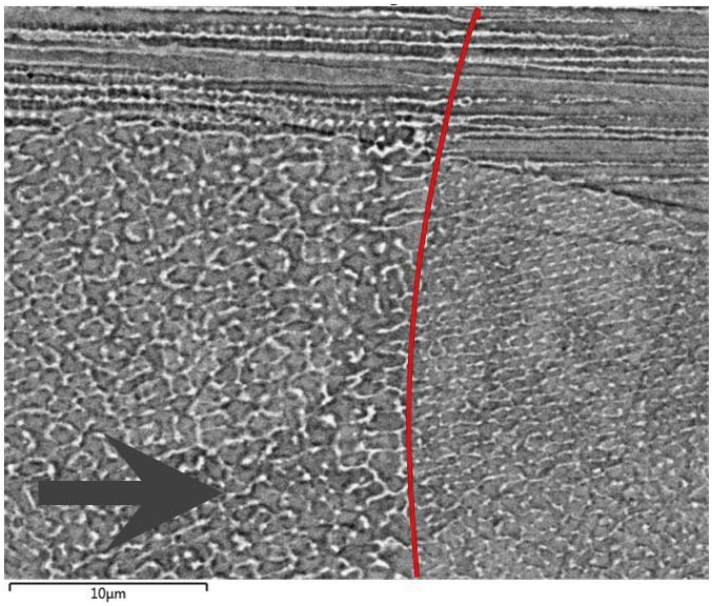


Figure 6 SEM micrograph of variation in as-built microstructure across a melt pool boundary, illustrating the change in size/granularity of the segregated phase across either side of the melt pool. An approximate boundary for the regions has been added in the form of a red curve. The arrow denotes build direction.

Similar grain elongation and pool contrast effects have been observed in other materials produced by AM methods (e.g., Ti-6Al-4V in [18]), suggesting that these effects may be present in other material systems which experience a similar thermal history in the course of additive manufacturing, as any additive metals process requires the rapid cooling of small liquid regions, which are prone to epitaxial growth from the underlying substrate. It remains to be seen if these segregation phenomena can be tailored or optimized for any particular purpose, though their scale and distribution suggest that they will be more readily driven back into solution than the more gross segregation which cast Inconel 718 presents [15].

### 3.2. Microstructure of Heat Treated Material

After solution annealing and aging treatments, the microstructure of PBF Inconel 718 improves dramatically, adopting much of the character of wrought material even though some anisotropy remains. Figure 7 is a dark-field optical micrograph showing both the in-plane and

out-of-plane grain structure for a sample that has undergone solution annealing and aging. All signs of the melt-pool contrast have been removed, indicating that the segregation phase has been driven back into solution completely. The contrast present is indicative of grain boundary locations and provides a likely culprit for the persistent anisotropy observed with respect to build direction. SEM images at higher magnification in Figure 7b confirmed that the segragation phase seen in the as-built samples (see Figure 6) are dissolved into the solid solution. Grain boundaries are visible with a small amount of isolated grain boundary delta phases, as expected. As discussed in the literature, a small amount of isolated grain boundary delta phase helps to constrain grain growth while minimizing the possible hydrogen enbrittlement induced by excessive amount of grain boundary delta and acicular delta phase [5].

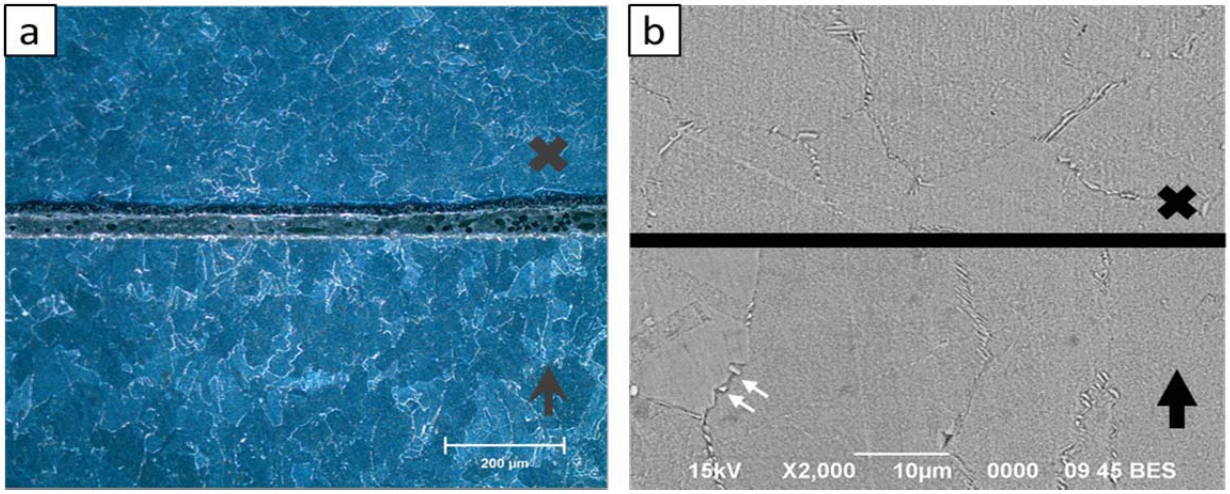


Figure 7: (a) Optical image of variation in grain shape as a function of orientation in samples with heat treatment without stress relief. Note that the elongation of grains in the build direction (denoted by black arrow) is significantly reduced as compared to the as-built state shown in Figure 5. (b) SEM images at higher magnification confirmed that the segregations seen in the as-built samples are driven back into the solution. A small amount of isolated grain boundary delta phases are visible (white arrows).

EBSD measurements illustrating the grain orientations of these microstructures can be seen in Figure 8, showing the absense of a strong texturing effect like that observed in the as-built material. It is clear that the grain elongation present in as-built material has been modified somewhat in heat treated material, although some elongation remains. This is most clear when comparing the X/Y plane and X/Z plane direct, as the X/Y plane shows a more uniform grain shape, while the X/Z plane appears somewhat columnar. This is supported by the mechanical property data shown in Figure 2, in which the orientation dependence of all of the mechanical properties is less severe in the heat treated material than in as-built material.

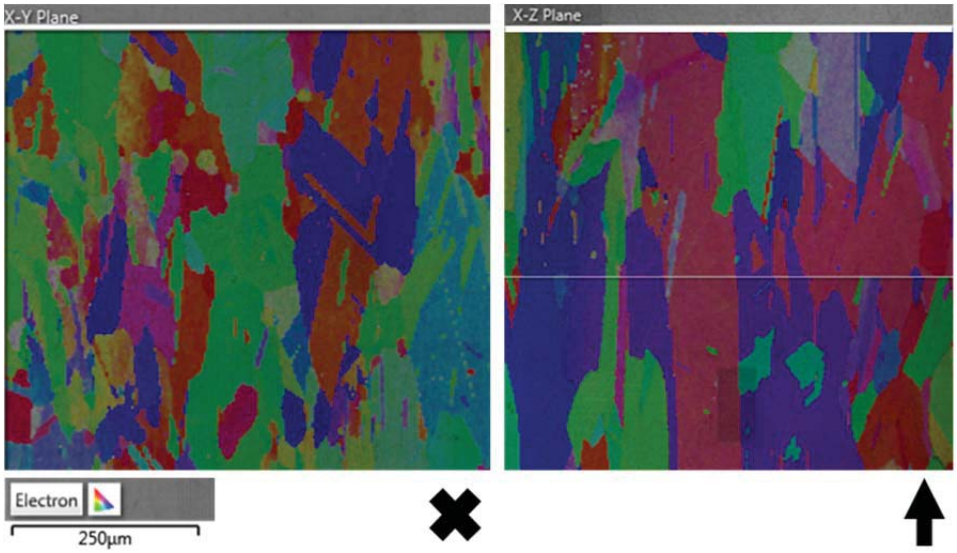


Figure 8: EBSD Map of heat treated sample showing that the as-built texturing is altered significantly through solution annealing and aging. Some elongation of grains in the Z-direction remain. Build orientation is indicated with an arrow, while the X denotes samples viewed within the build plane.

## 3.3. Comparing Wrought and PBF Microstructures

As mentioned in literature, the distribution of delta phase is one of the key differences between aerospace and oilfield grades of Inconel 718, as oilfield material sacrifices the high temperature creep properties associated with grain boundary decoration by delta phase particles for an enhanced resistance to hydrogen embrittlement associated with the absence of substantial grain boundary delta phase [5]. In other words, aerospace applications like the delta phase while oil and gas applications avoid it. In comparison to wrought Inconel 718 produced for oilfield applications (see example in Figure 9a), the local microstructure of treated PBF material appears very similar with the exception of the grain size/shape, as shown in Figure 9b. As with the wrought material, accumulation of the delta phase is observed in some isolated grain boundaries (see Figure 7b), but it is not pervasively distributed.

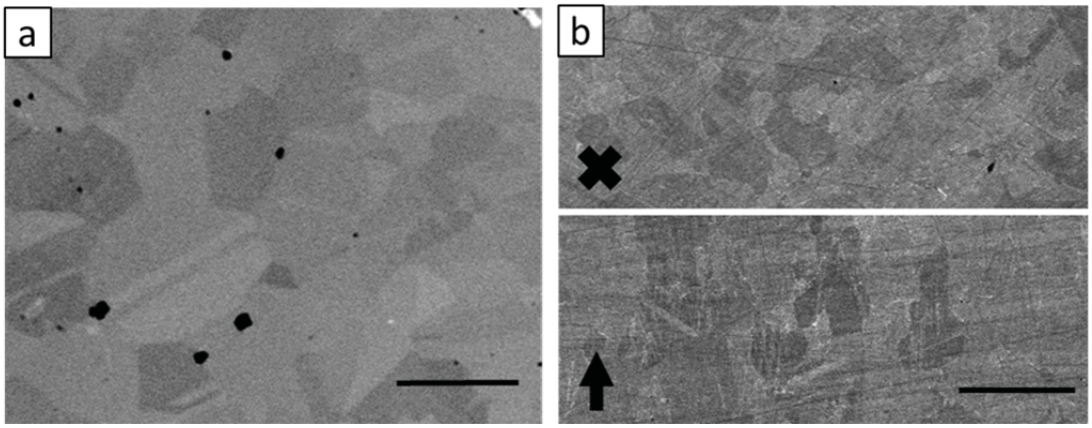


Figure 9: SEM images of the microstructure of (a) wrought Inconel 718 and (b) PBF Inconel 718 where the build orientation is indicated with an arrow: X denotes samples viewed within the build plane. Both the wrought and PBF samples are solution annealed and aged. Scale bar = 100 µm.

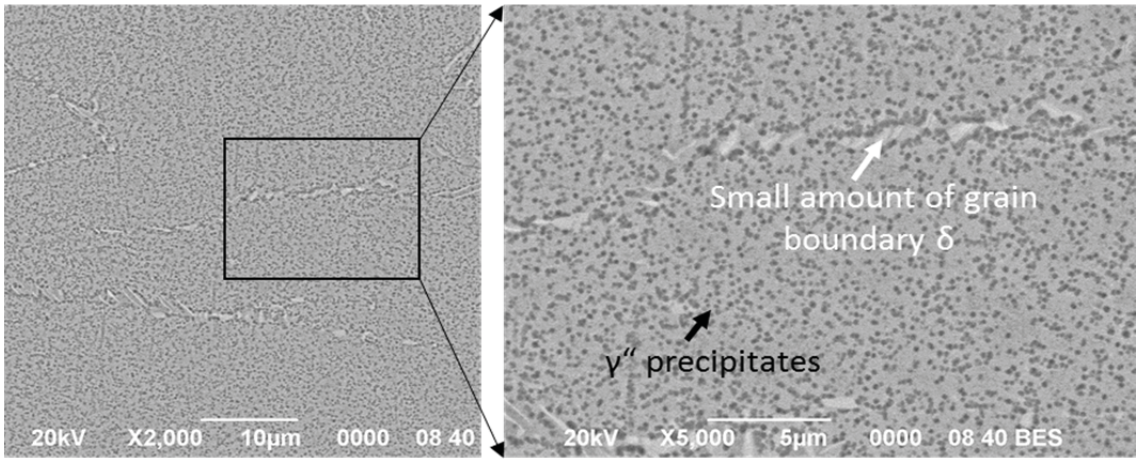


Figure 10: SEM images of the precipitations in PBF Inconel 718 after solution annealing and aging. Major strengthening γ" precipitations are observed in the alloy matrix as noted in zoomed-in region; a small amount of globular δ precipitations are formed along grain boundaries.

Further microstructure observation supports the hypothesis that the improvement in mechanical properties following heat treatment is due primarily to the refinement of local microstructure (both by driving Laves phases back into solution, as well as through precipitation of γ′′), and that the local microstructure meets the expectations of sour service applications, as shown in Figure 10. Some grain elongation remains present even in heat treated material, accounting for the residual mechanical anisotropy observed.

## 4. Summary and Future Work

In this work, Inconel 718 has been produced using a laser-based powder bed fusion (PBF) additive manufacturing process, and the as-deposited microstructure and orientation has been studied. Under the applied heat treatment conditions, mechanical and microstructural properties that met the minimum specification were obtained. This work also demonstrates that the anisotropy in Inconel 718 parts produced using laser-based PBF is not entirely removed by subsequent heat treatments, and it may be an artifact of the as-deposited grain structure, whose elongated grains may stretch through several melt pools. The as-built material is observed to exhibit some texturing, with (001) being the preferential growth direction. Despite some residual anisotropy, heat treatments are sufficient to provide material qualities within specification, even without the use of HIP (hot isostatic pressing). These results provide a positive first step toward process qualification for AM metal parts and suggest that laser-based PBF materials merit further study for applications traditionally satisfied by wrought material, as any segregation phenomena present are limited in size due to the rapid cooling rates of the melt pools. This suggests that PBF materials will be more amenable to microstructural refinement through post-processing heat treatments than traditional cast parts, potentially across a variety of material systems. Additional efforts will be required to assess the corrosion behaviors of laser-based PBF Inconel 718 and to determine its ultimate suitability for oilfield applications, as the effects of $CO_2$ and $H_2S$ corrosion on PBF/DMLS materials have not yet been investigated. As prior application of superalloy 718 for sour service required tight composition controls [4], it may be that the currently available PBF feedstock powders may be further optimized in terms of composition.

## Acknowledgments

We gratefully acknowledge funding from Schlumberger-Doll Research for this study. Any opinions, findings, and conclusions or recommendations presented in this paper are those of the authors and do not necessarily represent the views of Schlumberger-Doll Research.

## References

[1] Fulcher, B. and Leigh, D. K., 2013, *Metals Additive Manufacturing Development at Harvest Technologies*, 24th Annual International Solid Freeform Fabrication Symposium. University of Texas - Austin, 408-423, http://sffsymposium.engr.utexas.edu/Manuscripts/2013/2013-32-Fulcher.pdf.

[2] Gratton, A., 2012, "Comparison of Mechanical, Metallurgical Properties of 17-4PH Stainless Steel between Direct Metal Laser Sintering (DMLS) and Traditional Manufacturing Methods", *Proceedings of the National Conference of Undergraduate Research* UNC Asheville.

[3] SpaceX, 2014, "SpaceX Launches 3D-Printed Part to Space, Creates Printed Engine Chamber," http://www.spacex.com/news/2014/07/31/spacex-launches-3d-printed-part-space-creates-printed-engine-chamber-crewed, Retrieved January 5, 2016.

[4] Bhavsar, R. B., Collins, A. and Silverman, S., 2001, "Use of Alloy 718 and 725 in Oil and Gas Industry", *Superalloys 718, 625, 706 and Various Derivatives*, Loria, E. A., The Minerals, Metals, and Materials Society (TMS), 47-55, http://www.tms.org/superalloys/10.7449/2001/Superalloys_2001_47_55.pdf.

[5] DeBarbadillo, J. J. and Mannan, S. K., 2012, "Alloy 718 for Oilfield Applications," *JOM*, 64(2), 265-270.

[6] API, 2015, *Age-Hardened Nickel-Based Alloys for Oil and Gas Drilling and Production Equipment*, Association of Petroleum Industry (API), API Standard 6A718, http://mycommittees.api.org/standards/ecs/sc6/Commitee%20Documents/6A718%20draft%20September%202013%20without%20Annex.pdf.

[7] Xu, J., John, H., Wiese, G. and Liu, X., 2010, "Oil-Grade Alloy 718 in Oil Field Drilling Applications", *Superalloy 718 and Derivatives*, Ott, E. A., Groh, J. R., Banik, A., Dempster, I., Gabb, T. P., Helmink, R., Liu, X., Mitchell, A., Sjöberg, G. P. S. and Wusatowska-Sarnek, A., John Wiley & Sons, Hoboken, NJ, 521–537.

[8] Wang, Z., Guan, K., Gao, M., Li, X., Chen, X. and Zeng, X., 2012, "The Microstructure and Mechanical Properties of Deposited-IN718 by Selective Laser Melting," *Journal of Alloys and Compounds*, 513, 518-523.

[9] Jia, Q. and Gu, D., 2014, "Selective Laser Melting Additive Manufacturing of Inconel 718 Superalloy Parts: Densification, Microstructure and Properties," *Journal of Alloys and Compounds*, 585, 713-721.

[10] Amato, K. N., Gaytan, S. M., Murr, L. E., Martinez, E., Shindo, P. W., Hernandez, J., Collins, S. and Medina, F., 2012, "Microstructures and Mechanical Behavior of Inconel 718 Fabricated by Selective Laser Melting," *Acta Materialia*, 60(5), 2229-2239.

[11] Sames, W. J., Unocic, K. A., Dehoff, R. R., Lolla, T. and Babu, S. S., 2014, "Thermal Effects on Microstructural Heterogeneity of Inconel 718 Materials Fabricated by Electron Beam Melting," *Journal of Materials Research*, 29(17), 1920-1930.

[12] Strondl, A., Fischer, R., Frommeyer, G. and Schneider, A., 2008, "Investigations of MX and γ'/γ'' precipitates in the Nickel-based Superalloy 718 Produced by Electron Beam Melting," *Materials Science and Engineering A*, 480(1-2), 138-147.

[13] Dehoff, R. R., Kirka, M. M., Sames, W. J., Bilheux, H., Tremsin, A. S., Lowe, L. E. and Babu, S. S., 2015, "Site Specific Control of Crystallographic Grain Orientation through Electron Beam Additive Manufacturing," *Materials Science and Technology*, 31(8), 931-938.

[14] Carlson, R. G. and Radavich, J. F., 1989, "Microstructural Characterization of Cast 718", *Superalloy 718 - Metallurgy and Applications*, Loria, E. A., The Minerals, Metals, and Materials Society (TMS), 79-95, http://www.tms.org/superalloys/10.7449/1989/Superalloys_1989_79_95.pdf.

[15] Radavich, J. F., 1989, "The Physical Metallurgy of Cast and Wrought Alloy 718", *Superalloys 718. 625. 706 and Various Derivatives*, Loria, E. A., The Minerals, Metals, and Materials Society (TMS), 229-240, http://www.silencertalk.com/docs/01-0970-229.pdf.

[16] Blackwell, P. L., 2005, "The Mechanical and Microstructural Characteristics of Laser-Deposited IN718," *Journal of Materials Processing Technology*, 170(1-2), 240-246.

[17] Chang, K.-M., Lai, H.-J. and Hwang, J.-Y., 1994, "Existence of Laves Phase in Nb-Hardened Superalloys", *Superalloys 718, 625, 706 and Various Derivatives*, Loria, E. A., The Minerals, Metals, and Materials Society (TMS), 683-694, http://www.tms.org/superalloys/10.7449/1994/Superalloys_1994_683_694.pdf.

[18] Carroll, B. E., Palmer, T. A. and Beese, A. M., 2015, "Anisotropic Tensile Behavior of Ti–6Al–4V Components Fabricated with Directed Energy Deposition Additive Manufacturing," *Acta Materialia*, 87, 309-320.